

Deriving Metallicity and Atmospheric Parameters for the Fast-Rotating SB2 Binary HIP 103833: Addressing Challenges in Close Binary Spectroscopy

Noriyuki KATOH ¹

¹*Graduate School of Human Development and Environment, Kobe University,
3-11 Tsurukabuto, Nada-ku, Kobe-shi, Hyogo 657-8501, Japan
noriyuki.k@panda.kobe-u.ac.jp*

(Received 2024 October 31; accepted 2024 November 21)

Abstract

The spectrum of a close binary star is a composite of the spectra of both the primary and secondary stars. Furthermore, high stellar rotational velocities lead to the blending of absorption lines, which complicates the accurate measurement of equivalent widths. In this study, we focused on the SB2 spectroscopic binary HIP 103833, for which the atmospheric parameters (effective temperature, surface gravity) and stellar parameters (mass, radius, luminosity) are already established. Utilizing spectral data obtained from the Nayuta Telescope at Nishi-Harima Observatory and MALLS, we derived atmospheric parameters and metallicities based on the equivalent widths of iron absorption lines. The parameters obtained in this research closely align with those from previous studies, thereby supporting the reliability of our equivalent width measurements. Additionally, the stellar parameters derived from our atmospheric analysis are not expected to differ significantly from those obtained from orbital motions in previous studies.

Key words: stars: abundances — binaries: close — techniques: spectroscopic

1. Introduction

Stars that originate from the same molecular cloud tend to exhibit similar atmospheric chemical compositions, reflecting the cloud's initial chemical makeup. Observations, for instance, have confirmed that stars within young clusters exhibit comparable metallicities in their atmospheres (Paulson et al. 2003). Similarly, binary stars formed from a common molecular cloud core have been shown in previous studies to display metallicity differences of no more than 2% between their primary and secondary stars (Takeda 2005).

However, there are reports of binary stars exhibiting significant differences in metallicity. For instance, in binary systems where one star hosts exoplanets while the other does not, the planet-hosting star typically demonstrates a higher metallicity (Liu et al. 2018). Furthermore, studies have indicated a correlation between the separation of binary stars and the variation in their metallicity; Ramírez et al. (2019) found that larger separations are associated with greater disparities in metallicity. This trend has been interpreted as a potential reflection of inhomogeneous metallicity distributions within molecular cloud cores.

Recent models of binary star formation suggest that the strength of the magnetic field and the rotational velocity of a molecular cloud core influence whether it undergoes macro-scale (~ 100 AU) or micro-scale (~ 10 AU) splitting (Machida 2010). Macro-scale splitting is more likely to produce binary systems with considerable separations and potentially distinct metallicities due to the partitioning of regions with varying compositions. In contrast, micro-scale splitting is expected

to occur within regions of similar metallicities, making it unlikely for close binary stars to exhibit significant discrepancies in metallicity.

In close binaries with high rotational velocities, the blending of the composite spectrum and nearby absorption lines presents challenges for accurately determining the atmospheric parameters of each star. Given these difficulties, we focus on HIP 103833, a close and eclipsing binary system. The orbital motion and photometric data for HIP 103833 have yielded reliable mass estimates for both stars, and atmospheric parameters have already been calculated (e.g., Kjurkchieva et al. 2003; Luck 2017; Eker et al. 2018). This study aims to determine the atmospheric parameters and metallicities of the primary and secondary stars in the HIP 103833 system from its spectral data and to derive the metallicity difference. We also discuss the criteria for assessing whether the observed difference in metallicity is significant.

2. Observations and Data Reduction

2.1. Target Binary and Observation

The observed binary star, HIP 103833 (also known as ER Vulpeculae, HD 200391, GAIADR3 1845206534070618624), is classified as a double-lined spectroscopic binary (SB2). The magnitudes and spectral types of the primary and secondary stars are 7.27 mag and 7.49 mag in the *V*-band, corresponding to spectral types G0V and G5V, respectively. Northcott & Bakos (1956) measured the radial velocities of this binary system to determine its orbital motion. The orbital elements are listed in table 1.

To obtain spectral data for the target binary, we conducted spectroscopic observations using the 2.0 m Nayuta Telescope at the Nishi-Harima Astronomical Observatory, University of Hyogo, employing the Medium And Low-dispersion Long-slit Spectrograph (MALLS) in the visible spectrum. As of April 2019, MALLS was equipped with an echelle mode. Observations were performed on 5 October 2021, from 11:50 to 16:50 (UTC). MALLS was operated in echelle mode to observe spectra in the wavelength range of 4960–6800 Å, with a spectral resolution of $R \sim 35,000$. The exposure time was set to 900 seconds per exposure, chosen to ensure that the wavelength shift due to binary orbital motion would not exceed the spectral resolution of approximately 0.168 Å at the center of the observed wavelength range. For a G-type main-sequence star with a magnitude of $V = 7.5$, a 900-second integration provided spectral data with a typical signal-to-noise ratio (S/N) of ~ 40 . We obtained 8 spectra, which were reduced using the IRAF software package in the standard manner. The data were processed within the spectral range of 5000–6600 Å. The observed spectrum within the range of 5610 to 5690 Å is presented in figure 1. This range corresponds to one of several orders in the echelle spectrum.

Table 1. Orbital elements of HIP 103833.

Period [day], P	0.6981
Periastron time, T_0 (JD-2,400,000.0)	33130.752
Eccentricity, e	0.02
omega primary, ω [deg.]	62.6
$K1$ [(km s $^{-1}$)]	138.5
$K2$ [(km s $^{-1}$)]	149.3
$V0$ [(km s $^{-1}$)]	25.2

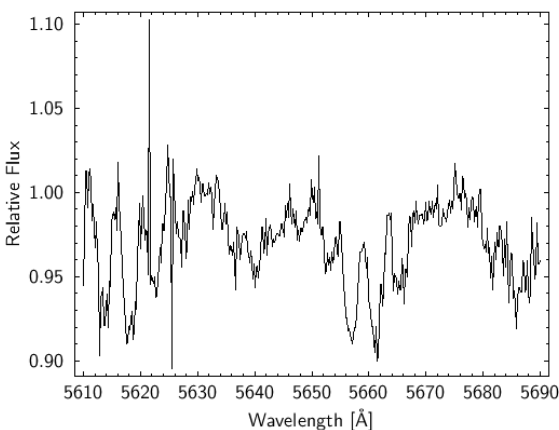


Fig. 1. The observed spectrum of HIP 103833. The vertical and horizontal axes represent the relative flux and wavelength, respectively. This spectrum corresponds to one of several orders in the echelle spectrum.

2.2. Measurement of Radial Velocity

We measured the radial velocities of the blue- and red-shifted stars from the 8 spectra. For these spectra, we utilized 10 Fe I absorption lines within the wavelength range of 5300–5700 Å, ensuring that there were no nearby strong absorption lines. The central wavelengths of each absorption line were determined using Gaussian fitting, and the wavelength shifts were calculated relative to the standard wavelengths. These shifts were then employed to calculate the radial velocities at each standard wavelength. Finally, the average of the 10 calculated velocities was taken as the measured radial velocity, with the variation among these values considered as the measurement error.

2.3. Measurement of Equivalent Widths

The S/N of the obtained spectra was insufficient for precise measurement of the equivalent widths. To enhance the S/N , 3 spectra with similar wavelength shifts were co-added, resulting in a synthesized spectrum with approximately double the original S/N . Equivalent widths for Fe absorption lines were measured from this synthesized spectrum using SPTOOL (Takeda 1995; Takeda et al. 2002) for 94 Fe I and 27 Fe II lines within the wavelength range of 5080–6600 Å.

Since HIP 103833 has a high rotational velocity of approximately 100 km s $^{-1}$ (Frasca et al. 2018), nearby absorption lines blend, complicating precise measurements. To address this issue, a model spectrum was generated to approximate the observed spectrum within the specified range, and iron abundances were derived from the absorption lines in that range. Based on these abundances, equivalent widths were determined through the following steps:

1. The MPFIT program in SPTOOL was utilized to determine the iron abundance by fitting approximate model spectra to several selected strong absorption lines within the specified wavelength range of the synthetic spectrum.
2. Using the WIDTH program in SPTOOL, the iron abundance was calculated for the line identified in Step 1 by varying the equivalent width from 1.0 to 100 mÅ in increments of 0.5 mÅ.
3. When the derived Fe abundance in Step 2 closely matched the Fe abundance from Step 1, the corresponding equivalent width value was recorded as the measured equivalent width.

As HIP 103833 is a double-lined spectroscopic binary (SB2), some absorption lines could not provide accurate equivalent widths. Luck (2017) indicates that the Fe abundance of HIP 103833 is $A(\text{Fe}) = 7.65 \pm 0.10$, which is close to solar levels. Therefore, in this study, the equivalent widths were deemed accurate when the derived Fe abundances fell within the range of $A(\text{Fe}) = 7.0\text{--}8.0$.

3. Results

3.1. Discrimination between the Primary and Secondary Stars

In this study, 8 radial velocity measurements were obtained for both the blue- and red-shifted stars (see table 2) and fitted

to the radial velocity curve using Exo-Striker exoplanet toolbox¹. The orbital elements of the HIP 103833 system were held constant. The radial velocities and the velocity curves are presented in figure 2.

The amplitude of the radial velocity was determined to be $K_1 = 138.5 \text{ km s}^{-1}$ for the blue-shifted star and $K_2 = 149.3 \text{ km s}^{-1}$ for the red-shifted star. Based on these results, the blue-shifted star was identified as the primary star, HIP 103833 A, while the red-shifted star was identified as the secondary star, HIP 103833 B.

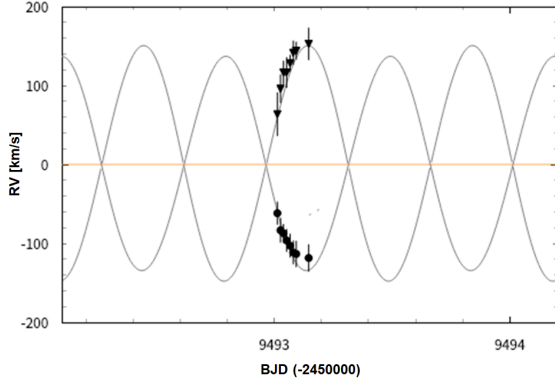


Fig. 2. The radial velocity of HIP 103833. The vertical and horizontal axes represent the radial velocity and Barycentric Julian Date, respectively. The radial velocities of the blue-shifted are indicated by filled circles, while those of the red-shifted stars are represented by filled triangles. The solid lines depict the variations in radial velocity calculated from the previously determined orbital elements.

3.2. Determination of Atmospheric Parameters

The equivalent widths of HIP 103833 were measured for 33 Fe I absorption lines and 8 Fe II absorption lines from the primary star, as well as for 23 Fe I absorption lines and 14 Fe II absorption lines from the secondary star. The rotational velocities were derived from 33 Fe I absorption lines and 8 Fe II absorption lines for the primary star, and from 20 Fe I absorption lines and 13 Fe II absorption lines for the secondary star. The equivalent widths and rotational velocities for each absorption line are presented in table 3.

The rotational velocities of the primary star, V_1 , and the secondary star, V_2 , were calculated as the averages of the rotational velocities derived from each absorption line, with the deviation from these averages considered as the measurement error. Consequently, V_1 and V_2 were determined to be $94.4 \pm 10.1 \text{ km s}^{-1}$ and $95.2 \pm 9.6 \text{ km s}^{-1}$, respectively. These values are comparable to those reported in previous studies (Frasca et al. 2018).

For the analysis of atmospheric parameters (effective temperature T_{eff} , surface gravity $\log g$, and microturbulence velocity ν), absorption lines with equivalent widths ranging from 5 to 100 mÅ were utilized. The WIDTH program in SPTOOL was employed to derive solutions for the atmospheric parameters, using atomic line data and the equivalent widths of the absorption lines as constants, while simultaneously satisfying

the following criteria:

- The iron abundances derived from Fe I absorption lines exhibit no dependence on the excitation potential, χ .
- The mean iron abundance derived from Fe I absorption lines is equal to the mean iron abundance derived from Fe II absorption lines.
- The iron abundances derived from Fe I absorption lines are independent of the equivalent widths.

The measurement errors for the atmospheric parameters were estimated based on the standard deviation of the iron abundance. For instance, in the case of effective temperature, the mean and standard deviation of the iron abundance are derived by assuming an effective temperature and calculating the iron abundance for each iron absorption line using the WIDTH program. Subsequently, the effective temperature is adjusted in increments of 10 K, and the mean iron abundance is recalculated at each step. The largest change in effective temperature that still results in a mean iron abundance variation within the standard deviation is considered the measurement error for the effective temperature. Similarly, surface gravity and microturbulence velocity were varied in increments of 0.01 cm s^{-2} and 0.1 m s^{-1} , respectively. The determined atmospheric parameters are presented in table 4.

3.3. Determination of Metallicity

Using the equivalent widths of the iron absorption lines and the determined atmospheric parameters, we calculated the iron abundance for each absorption line using the WIDTH program. The mean value of these calculations was adopted as the iron abundance for each star, while the standard deviation was considered the measurement error. Consequently, we determined the iron abundance to be $A(\text{Fe})_A = 7.41 \pm 0.24$ for the primary star and $A(\text{Fe})_B = 7.71 \pm 0.20$ for the secondary star. The solar iron abundance is given as $A(\text{Fe})_{\odot} = 7.50$ (Asplund et al. 2009). Therefore, the metallicity of the primary and secondary stars was derived as $[\text{Fe}/\text{H}]_A = -0.005 \pm 0.014 \text{ dex}$ and $[\text{Fe}/\text{H}]_B = 0.012 \pm 0.011 \text{ dex}$, respectively.

4. Discussion

The rotational velocities, derived from iron absorption lines in our spectral data, are consistent with previous measurements. Our atmospheric parameters (see table 4), based on equivalent width measurements of Fe I and Fe II, are also comparable to those from previous research. These findings suggest minimal measurement uncertainty.

4.1. Equivalent Width Differences and Metallicity Differences

Katoh (2019) indicated that in equal-mass binaries, variations in the equivalent widths of identical absorption lines between the primary and secondary stars reflect differences in their stellar compositions. For HIP 103833, the equivalent widths of 10 Fe I absorption lines and 3 Fe II absorption lines, which were measurable for both the primary and secondary stars, are presented in figure 3.

¹ Exo-Striker exoplanet toolbox (<https://github.com/3fon3fonov/exostriker>)

Table 2. Radial Velocities of the blue- and red-shifted stars.

BJD-UTC* (-2450000)	Blue-shifted RV [km s ⁻¹]	Uncertainty [km s ⁻¹]	Red-shifted RV [km s ⁻¹]	Uncertainty [km s ⁻¹]
9493.01614	-61.7	13.8	63.6	26.9
9493.02954	-83.4	15.0	96.0	17.3
9493.04228	-87.3	11.0	116.4	14.2
9493.05530	-96.3	13.7	116.4	18.7
9493.07015	-102.9	14.3	128.3	9.7
9493.08366	-111.5	14.4	141.5	14.6
9493.09631	-113.4	16.0	144.1	10.6
9493.14929	-118.5	16.6	152.8	19.8

*We converted HJD to BJD-UTC using the calculation code provided by Eastman, Siverd, and Gaudi (2010).

The equivalent widths of the primary star and the secondary star are denoted as EW_A and EW_B , respectively. The average difference in equivalent widths is given by $EW_A - EW_B = -9.35 \pm 10.73 \text{ \AA}$. The equivalent widths of the secondary star are greater than those of the primary star. Additionally, the difference in iron abundance is more pronounced in the secondary star, with $[\text{Fe}/\text{H}]_A - [\text{Fe}/\text{H}]_B = -0.017 \pm 0.025$ dex, suggesting that the secondary star is more metal-rich.

However, the uncertainties in both the equivalent width differences and the compositional variations suggest that there is no definitive evidence of a significant difference in iron abundance between the primary star and the secondary star. Consequently, this study does not exclude the possibility that the iron compositions of HIP 103833 A and HIP 103833 B are similar. Additionally, metallicities typically vary by approximately 10% among stars within an open cluster (Paulson et al. 2003). The iron abundances between HIP 103833 A and HIP 103833 B also differ by only about 10% at most. Therefore, even if the metallicity difference is significant, it would not necessarily be unique.

4.2. Characterization of Binary Stars

The stellar masses, radii, and luminosities of HIP 103833 A and HIP 103833 B were determined using EXOFAST (Eastman et al. 2013), which calculates stellar parameters based on our atmospheric parameters. For error estimation, only the effective temperature was treated as a variable. The derived parameters are shown in table 5.

The masses of the primary star and the secondary star are $M_1 = 1.25 \pm 0.09 M_\odot$ and $M_2 = 1.16 \pm 0.07 M_\odot$, respectively. Consequently, the mass ratio is given by $q = (M_2/M_1) = 0.928$. The mass ratio of the binary system can also be derived from the radial velocity amplitudes, denoted as K . The radial velocity amplitudes of the primary and secondary stars are represented as K_1 and K_2 , respectively. Thus, the mass ratio can be expressed as $q = K_1/K_2$. The mass ratio derived from the radial velocity amplitudes is 0.928, which is consistent with the mass ratio obtained from the stellar composition. Regarding

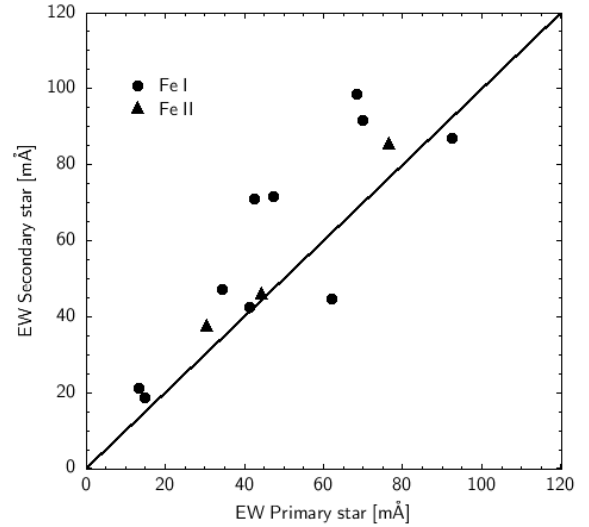


Fig. 3. Equivalent widths of the primary and secondary stars in HIP 103833. The horizontal axis represents the equivalent widths of the primary star, while the vertical axis represents the equivalent widths of the secondary star. The filled circles indicate the observed equivalent widths of Fe I lines, and the filled triangles represent the observed equivalent widths of Fe II lines. The solid line illustrates that the two quantities are equal.

the radii and luminosities, the primary star has a radius of $R_1 = 1.80 \pm 0.07 R_\odot$ and a luminosity of $L_1 = 3.54 \pm 1.01 L_\odot$, while the secondary star has a radius of $R_2 = 1.19 \pm 0.04 R_\odot$ and a luminosity of $L_2 = 1.74 \pm 0.40 L_\odot$.

Kjurkchieva, Marchev, and Zola (2003) determined the orbital inclination i of HIP 103833 AB to be $66^\circ.1$ based on photometric observations of the system as an eclipsing binary. Consequently, they calculated the mass of the primary star, $M_1 = 1.16 \pm 0.04 M_\odot$, and the mass of the secondary star, $M_2 = 1.05 \pm 0.04 M_\odot$, from the orbital elements, including the inclination. The orbital inclination and the semi-major axis of the binary system provide the relative radii of the primary and

secondary stars. As a result, the radii of the primary star, $R_1 = 1.25 \pm 0.05 R_\odot$, and the secondary star, $R_2 = 1.12 \pm 0.16 R_\odot$, were derived. Yakut and Eggleton (2005) utilized these radii to estimate the luminosities of the primary star, $L_1 = 1.81 L_\odot$, and the secondary star, $L_2 = 1.04 L_\odot$.

In this study, the stellar masses, radii, and luminosities derived from the atmospheric parameters are not expected to differ significantly from those obtained from the orbital motions in the previous study.

4.3. Age of the Target Binary

For HIP 103833, for which the primary and secondary effective temperatures and luminosities have been determined, we estimate the age of the system using the H-R diagrams and the Padova evolutionary tracks (Marigo et al. 2008). These evolutionary tracks calculate the isochrones from the zero-age main sequence (ZAMS) up to 13.5 Gyr. H-R diagram for the target binary is presented in figure 4. The positions of the primary and secondary stars coincide with the 5.0–7.0 Gyr isochrones. Casagrande et al. (2011) estimated the age of the system to be between 5.02 and 9.43 Gyr, with a maximum likelihood age of 7.90 Gyr, which is consistent with our estimated age.

Some previous studies have estimated the age of HIP 103833 to be 9.2 Gyr (Feltzing et al. 2001) and 10.3 Gyr (Luck 2017). This binary system may be in an advanced stage of evolution. In this study, the primary star is cooler than the secondary star; however, its radius and luminosity are approximately 1.5 and 2 times larger, respectively. The position of the primary star on the H-R diagram appears to be farther from the main sequence, suggesting that the primary star may be evolving off the main sequence.

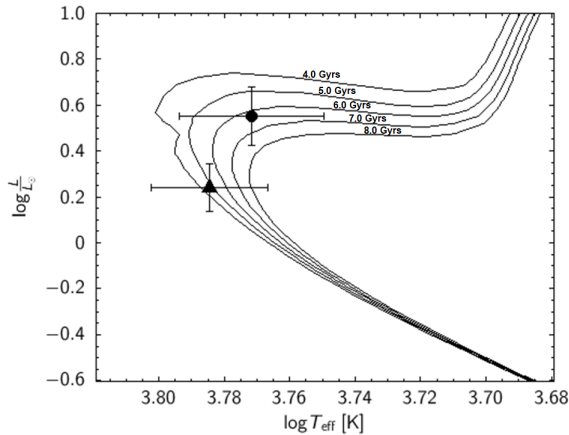


Fig. 4. H-R diagram of HIP 103833. The vertical axis represents normalized luminosity on a logarithmic scale, while the horizontal axis represents effective temperatures, also on a logarithmic scale. The primary stars are plotted as filled circles, and the secondary stars are represented by filled triangles. The solid lines indicate the isochrones derived by Marigo et al. (2008).

5. Conclusion

In close binary systems, the overlapping spectra of the primary and secondary stars make it challenging to accu-

rately measure the equivalent widths of their absorption lines. Consequently, it is often unclear whether any observed differences in metallicity between the two stars are statistically significant. In this study, we focused on HIP 103833, a system for which the masses and atmospheric parameters of both stars have been derived from orbital motions and photometric data. We obtained spectral data of the binary using the Nayuta Telescope at the Nishi-Harima Astronomical Observatory and the MALLS, and we measured the Fe equivalent widths. This study derived the atmospheric parameters of the binary from the observed equivalent widths.

For these spectral data, we measured the radial velocities of the primary and secondary stars, identifying their individual spectra. The rotational velocities, derived from iron absorption lines, were $V_1 = 94.4 \pm 10.1 \text{ km s}^{-1}$ and $V_2 = 95.2 \pm 9.6 \text{ km s}^{-1}$, consistent with previous studies. Atmospheric parameters based on Fe I and Fe II equivalent width measurements were also comparable to those from previous research, suggesting minimal measurement uncertainty. Furthermore, the stellar mass, radius, and luminosity derived from our atmospheric parameters align with the values obtained from orbital motions in previous studies. Using the effective temperatures and luminosities, we constructed an H-R diagram and estimated the age of the binary system to be approximately 5.0 to 7.0 Gyr based on the evolutionary track. The primary star in the HIP 103833 system may exhibit signs of evolving beyond the main sequence.

This study indicated that, even in SB2 spectroscopic binaries with high rotational velocities, metallicities can be accurately derived by measuring the Fe equivalent widths for the primary and secondary stars individually. We also discussed the significance of the metallicity differences in the HIP 103833 binary.

Acknowledgments

This research is based on data collected at the Nishi-Harima Astrophysical Observatory (NHAO), which is operated by the Center for Astronomy at the University of Hyogo. We would like to express our gratitude to all the staff members at NHAO for their support during the observations. In this study, the measurement of equivalent widths refers to the master's thesis of Mr. Hitoshi Funayama (Funayama 2007, Kobe University). This paper utilizes EXOFAST (Eastman et al. 2013), provided by the NASA Exoplanet Archive, which is managed by the California Institute of Technology under contract with the National Aeronautics and Space Administration as part of the Exoplanet Exploration Program. Additionally, this research employs TOPCAT, an interactive graphical viewer and editor for tabular data (Taylor 2005). We also utilized the SIMBAD database and the VizieR Service, both operated by the CDS in Strasbourg, France.

References

- Asplund, M., Grevesse, N., Sauval, A. J., & Scott, P. 2009, *ARA&A*, 47, 481
- Casagrande, L., Schönrich, R., Asplund, M., Cassisi, S., Ramírez, I., Meléndez, J., Bensby, T., & Feltzing, S. 2011, *A&A*, 530, 138
- Eker, Z., et al. 2018, *MNRAS*, 479, 5491

- Feltzing, S., Holmberg, J., & Hurley, J. R. 2001, *A&A*, 377, 911
- Frasca, A., Guillout, P., Klutsch, A., Freire Ferrero, R., Marilli, E., Biazzo, K., Gandolfi, D., & Montes, D. 2018, *A&A*, 612, A96
- Eastman, J., Siverd, R., & Gaudi, B. S. 2010, *PASP*, 122, 935
- Eastman, J., Gaudi, B. S., & Agol, E. 2013, *PASP*, 125, 83
- Katoh, N. 2019, *Stars and Galaxies*, 2, 2
- Kjurkchieva, D. P., Marchev, D. V., & Zola, S. 2003, *A&A*, 404, 611
- Liu, F., Yong, D., Asplund, M., Feltzing, S., Mustill, A. J., Meléndez, J., Ramírez, I., & Lin, J. 2018, *A&A*, 614, A138
- Luck, R. E. 2017, *AJ*, 153, 21
- Machida, M. N. 2010, in *IAU Symp. 270*, ed. A. Elmegreen & G. Trimble, 65
- Marigo, P., Girardi, L., Bressan, A., Groenewegen, M. A. T., Silva, L., & Granato, G. L. 2008, *A&A*, 482, 883
- Northcott, R. J., & Bakos, G. A. 1956, *AJ*61, 188
- Paulson, D. B., Sneden, C., & Cochran, W. D. 2003, *AJ*, 125, 3185
- Ramírez, I., Khanal, S., Lichon, S. J., Chanamé, J., Endl, M., Meléndez, J., & Lambert, D. L. 2019, *MNRAS*, 490, 2448
- Takeda, Y. 1995, *PASJ*, 47, 287
- Takeda, Y., Ohkubo, M., & Sadakane, K. 2002, *PASJ*, 54, 451
- Takeda, Y. 2005, *PASJ*, 57, 83
- Taylor, M. B. 2005, in *ASP Conf. Ser.*, 347, *Astronomical Data Analysis Software and Systems XIV*, ed. P. Shopbell et al. (San Francisco: ASP), 29
- Yakut, K., & Eggleton, P. P. 2005, *ApJ*, 629, 1055

Table 3. Equivalent widths and rotational velocities for the primary and secondary stars in HIP 103833.

λ [Å]	Primary star		Secondary star	
	EW [mÅ]*	V_{rot} [km s ⁻¹]*	EW [mÅ]*	V_{rot} [km s ⁻¹]*
	Line : Fe I			
5083.340	92.5	101.458	87.0	69.927
5198.700	82.5	90.026		
5225.533			65.5	120.373
5247.060	53.5	71.649		
5250.217	62.0	103.786	44.5	80.084
5253.500	70.0	88.700		
5322.050	43.5	70.581		
5326.145	44.5	98.631		
5330.000	36.0			
5412.788	13.5	109.891	21.0	81.781
5473.910			58.0	88.587
5525.600	35.5	86.554		
5569.600	83.0	126.055	92.0	94.724
5600.227	15.0	84.431	18.5	88.103
5661.348			22.0	91.160
5705.468	34.5			
5784.661	11.0	98.568		
5856.090			18.5	90.449
6056.010	66.0	108.526		
6079.010			32.0	99.443
6082.715			44.0	108.898
6136.600	85.0	92.894		
6137.000	34.5		47.0	88.875
6157.730	48.5	91.763		
6159.380	10.0	90.906		
6165.360	36.5			
6173.343	56.0	117.515		
6180.208	41.5	113.001	42.5	87.182
6200.320			39.5	87.671
6219.289	58.5	68.233		
6229.240	11.0	100.018		
6232.649	42.5		71.0	89.991
6240.652			40.5	97.673
6246.300	59.0	82.975		
6252.500	70.0	98.450	91.5	109.139

Table 3. (Continued.)

λ [Å]	Primary star		Secondary star	
	EW [mÅ]*	V_{rot} [km s ⁻¹]*	EW [mÅ]*	V_{rot} [km s ⁻¹]*
6265.141	82.5	99.217		
6336.800			63.0	103.088
6392.540	6.5	83.508		
6393.600	85.5			
6400.000		97.753		
6411.600		94.253		
6421.350	75.5	105.314		
6591.320			10.0	95.853
6592.930	68.5	87.260	98.5	
6593.880	47.5		71.5	
Line : Fe II				
5132.674			39.5	100.728
5136.800			13.0	116.461
5197.576	76.5	60.361	85.0	86.608
5264.790	35.5	92.054		
5325.560	55.5	95.960	47.0	98.138
5414.075			38.0	79.155
5425.259	44.5	105.718	45.5	81.809
5525.130	7.0	96.285		
5627.490			14.5	106.206
5991.380			39.5	87.897
6084.110	30.5	108.878	37.0	108.898
6149.250			57.0	114.875
6179.395			7.5	98.760
6238.392			46.0	97.673
6239.948			18.0	
6247.562			47.5	104.960
6416.928	29.0	94.551		
6456.391	69.5	94.076		

* The blank spaces in the EW and V_{rot} columns indicate values that could not be measured.

Table 4. Atmospheric Parameters and Metallicities of HIP 103833 A and B.

	HIP 103833 A	HIP 103833 B
Effective temperature, T_{eff} [K]	5910 ± 300	6090 ± 250
Surface gravity, $\log g$ [cm s^{-2}]	4.02 ± 0.70	4.35 ± 0.50
Microturbulence velocity, v [km s^{-1}]	0.4 ± 1.0	0.4 ± 0.9
Metallicity, [Fe/H] [dex]	-0.005 ± 0.014	0.012 ± 0.011

Table 5. Stellar Parameters of HIP 103833 binary.

	HIP 103833 A	HIP 103833 B
Mass [M_{\odot}]	1.25 ± 0.09	1.16 ± 0.07
Radius [R_{\odot}]	1.80 ± 0.07	1.19 ± 0.04
Luminosity [L_{\odot}]	3.54 ± 1.01	1.74 ± 0.40